

Novel pulse sequences for time-resolved photo-CIDNP

MARTIN GOEZ*[†], I. KUPROV[‡], K. HUN MOK[‡] and P. J. HORE[‡]

[†]Fachbereich Chemie, Martin-Luther-Universität Halle-Wittenberg,
Kurt-Mothes-Strasse 2, D-06120 Halle/Saale, Germany

[‡]Department of Chemistry, University of Oxford, Physical and Theoretical
Chemistry Laboratory, South Parks Road, Oxford OX1 3QZ, UK

(Received 14 October 2005; in final form 14 February 2006)

The properties of a new class of pulse sequences for photo-CIDNP (photochemically induced dynamic nuclear polarization) are analysed in detail, and guidelines for their optimization and applicability are derived. Sensitivity is a central problem with time-resolved photo-CIDNP experiments. By using multiple laser flashes per acquisition and storing the polarizations temporarily in the spin system, a significant improvement is achieved. An alternative application is the reduction of the absorbed light needed to attain a given sensitivity. Compared to conventional signal averaging with the same number n of flashes, a maximum additional improvement by a factor of slightly more than $0.5\sqrt{n}$ can be achieved in both cases. By an analysis of the transfer pathways, it is shown that multiplet signals and CIDNP multiplet effects can also be investigated in this way, even for strongly coupled spin systems. Experimental examples are given.

Keywords: Chemically induced dynamic nuclear polarization; NMR spectroscopy; Pulse sequences; Laser methods; Spin chemistry

1. Introduction

The CIDNP (chemically induced dynamic nuclear polarization) effect has been known for almost four decades [1, 2]. Within that time, photo-CIDNP spectroscopy [3] has developed into a powerful tool for the study of such diverse problems as molecular diffusion [4, 5], intramolecular motions [6, 7] and rearrangements [8, 9], mechanisms [10, 11] and kinetics [12, 13] of organic photoreactions, processes in the photosynthetic reaction centre [14, 15], and structures and folding of proteins [16, 17]. What makes CIDNP unique is that the polarizations are generated [18, 19] in the paramagnetic reaction intermediates (radical pairs or biradicals) on a timescale of nanoseconds to subnanoseconds, but are stored and accumulated in the diamagnetic reaction products, where the polarizations are essentially frozen for a time on the order of T_1 . Because of that peculiarity, time-resolved CIDNP experiments on a microsecond to submicrosecond timescale [20–25] are feasible even though kinetic processes amenable to NMR detection are normally many orders of magnitude slower.

Despite the fact that CIDNP spectroscopy has apparently reached a state of maturity, where its methodology and interpretation have largely become routine, we have recently developed novel pulse sequences [26] that considerably improve the performance of time-resolved CIDNP experiments, and have demonstrated the feasibility of these schemes experimentally. In this work, we will analyse their properties in depth, demonstrate their applicability to multiplet signals and CIDNP multiplet effects, and give details regarding their optimization. Their underlying idea, storing and accumulating magnetization in a spin system for later readout, is suggested by the CIDNP effect itself.

2. Experimental

For technical details of our time-resolved CIDNP equipment, see [27]. The experiments were carried out on a 600 MHz (14.1 T) Varian INOVA NMR spectrometer; the light source was a frequency tripled Spectra-Physics GCR-130 Nd:YAG laser (355 nm; flash duration, ca. 5 ns; flash energy, ca. 40 mJ). All chemicals were obtained commercially in the highest available purity and used as received.

*Corresponding author. Email: goez@chemie.uni-halle.de

3. Results and discussion

Figure 1 outlines the principle of a time-resolved photo-CIDNP experiment [28, 29]. A laser flash starts a photoreaction, the polarizations evolve during a variable delay Δt , and are then sampled by a radio frequency (rf) pulse. The time dependence of the polarizations is obtained from a series of experiments with different Δt . A typical laser flash is a few nanoseconds long, a typical rf pulse a few microseconds, and for the variable delay a time up to a millisecond covers the range that is probably most interesting because it is inaccessible by dynamic NMR. To make sure that the rf pulse samples only CIDNP and not the equilibrium magnetization, all that background is destroyed by presaturation before the laser flash. Relaxation during the short time Δt is usually negligible, so time-resolved CIDNP experiments rarely suffer from background problems.

There are a number of other attractive features to the experiment, such as the absence of lifetime broadening (because the stable products are observed) as well as paramagnetic broadening (because the radicals have disappeared when the free induction decay is recorded). However, there is also one severe disadvantage: only a small fraction of the molecules in the sample reacts, so the signal is often very small. The question of how the sensitivity can be improved is thus a key issue with time-resolved CIDNP.

The most straightforward approach would appear to be to increase the number of reacting molecules by using a higher laser power. However, there are several drawbacks. First, the cost of increasingly higher laser powers quickly becomes prohibitive, especially in view of the fact that the laser is the only additional large piece of equipment necessary to convert an existing NMR spectrometer into a time-resolved CIDNP setup. Second, optical components such as mirrors, prisms and/or lightguides are needed to get the light into the sample, and increasing the laser intensity above a certain threshold will result in damage to, or destruction of, these components. But the two most severe and

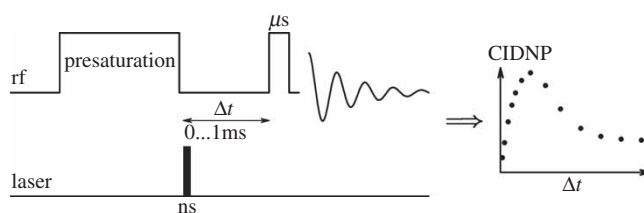


Figure 1. Principle of a time-resolved photo-CIDNP experiment. Shown is the timing of laser and rf pulses, and a schematic example of an experimental curve. Further explanation, see text.

fundamental problems are that high light intensities can open up completely new reaction channels, by two-photon processes [30, 31], and that they can distort the kinetics because second-order reactions that are negligible at the usual radical concentrations become dominant at high photon fluxes.

Signal co-addition, the approach extensively employed in all fields of NMR, will increase the sensitivity, as the signal increases linearly with the number n of scans but the noise only with the square root of that number. However, that approach is confronted with another problem: CIDNP experiments rely on chemical turnover, and most systems are not indefinitely photostable. Because the number of scans in a conventional CIDNP experiment is equal to the number of flashes, the signal increase is less than linear if decomposition occurs, but the noise is unchanged. So the sensitivity gain may become progressively smaller than \sqrt{n} .

The central problem of the usual co-addition approach is that the signal is stored and summed up *in the acquisition computer*, so each laser flash contributes not only a new signal but also—because it is followed by an acquisition—new noise. We have recently developed [26] a strategy to store and sum up CIDNP stemming from several laser flashes *in the spin system* itself, and to acquire only once, after such an accumulation. In that way, the noise is sampled only once, and the sensitivity should ideally increase linearly with the number of laser flashes.

The concept of storing a signal is not normally used in the context of CIDNP. However, even the basic time-resolved CIDNP experiment involves a storage process, as figure 2 illustrates. CIDNP is a time-dependent z magnetization. Left undisturbed, it would evolve after the first laser flash as depicted schematically by the dotted curve. An observation pulse applied at time Δt during that evolution period converts all or part of the CIDNP present at that very moment, $S(\Delta t)$, into transverse magnetization. The amount converted is determined by the flip angle; in the figure, we have assumed a $\pi/2$ pulse. Any subsequent time evolution of CIDNP (that is, of the z magnetization) has no influence whatsoever on the transverse magnetization, which precesses and persists for a time on the order of T_2 . In other words, CIDNP present at a given point of time can be stored in the transverse plane by an rf observation pulse.

Co-addition within the spin system becomes possible by the recognition that after such a period of *transverse storage* the signal can be restored to the z axis and, following an optional period of *longitudinal storage*, superimposed with CIDNP stemming from another flash. Putting the transverse signal back to the z axis

simultaneously destroys all CIDNP evolved in the meantime, $S(t_{\text{end}})$, as explained below. Another laser flash generates new CIDNP, and another observation pulse, applied at the same post-flash delay $\Delta t'$ as before, takes both the stored signal $S(\Delta t)$ and the new signal

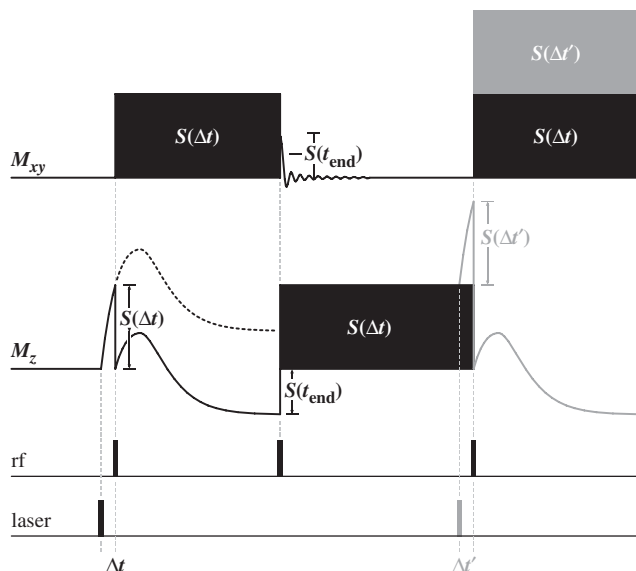


Figure 2. Storage of CIDNP in a multiflash experiment. Shown is the timing of the laser flashes and rf pulses, and the development of longitudinal and transverse magnetization M_z and M_{xy} . Further explanation, see text.

$S(\Delta t')$ into the transverse plane. From figure 2 it is evident that the alternation of transverse and longitudinal storage and the superposition of stored and new CIDNP can be repeated as often as desired.

The upper part of figure 3 gives details of our implementation of transverse storage [26]. In the basic version (rf pulse scheme, trace rf (a) only), a $\pi/2$ pulse initiates transverse storage. To eliminate differential precession, the transverse magnetization is refocused by a spin echo. As usual, pulse imperfections are compensated by a double spin echo (Carr–Purcell–Meiboom–Gill scheme [32, 33]). The last $\pi/2$ pulse of block S_1 restores the signal to the z axis. Simultaneously, it puts all CIDNP evolved in the meantime into the transverse plane, where it is destroyed by a strong z gradient.

If the observation pulse is not short on the timescale of CIDNP evolution, the stored signal is given by a convolution integral of pulse and kinetics [34]. Deconvolution methods can be applied [35], but for very fast reactions it might be desirable to use observation pulses with flip angles smaller than $\pi/2$ because they are shorter. This leads to a more sophisticated pulse scheme [26] (trace rf (b) replacing rf (a) as the only modification). The part S_1 after the laser pulse is the same as in the basic version except for the smaller flip angle α of the observation pulse. However, that pulse would only utilize a fraction of CIDNP previously stored, so it has to be preceded by an additional block S_0 . The first pulse of

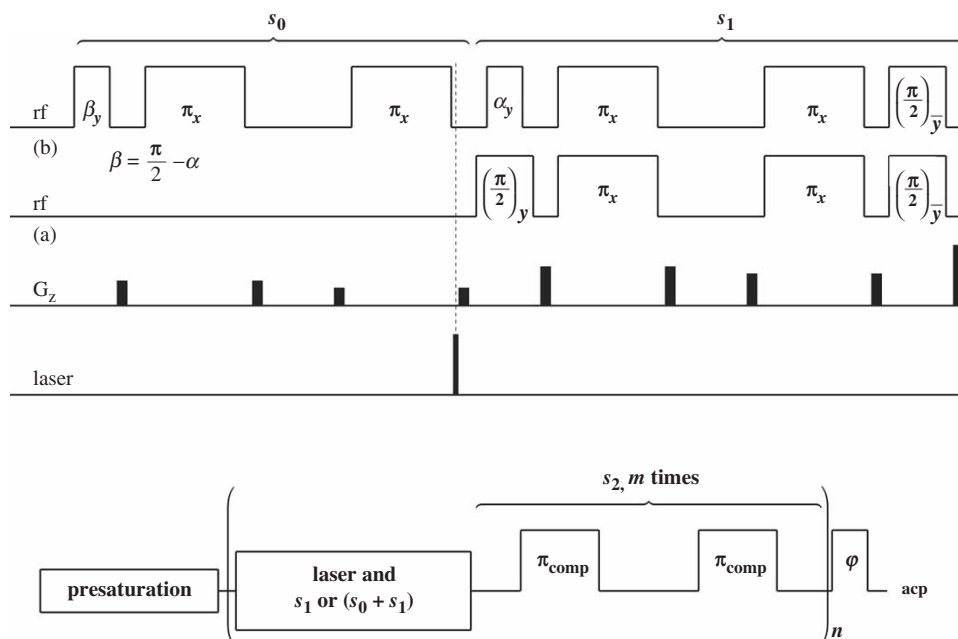


Figure 3. Implementation of time-resolved multiflash CIDNP experiments. Upper part, transverse storage. As rf pulse scheme, either rf (a) or rf (b) is used. The relative pulse phases are denoted by subscripts. G_z shows the field gradients. Lower part, longitudinal storage and readout. Further explanation, see text.

S_0 nutates CIDNP stored on z towards the transverse plane by the complementary angle β , $\beta = \pi/2 - \alpha$. Another double spin echo refocusses the transverse components at the moment of the observation pulse, which takes the stored signal the rest of the way into the transverse plane. Thus, no part of the stored signal is lost.

The chosen implementation of transverse storage, comprising either pulse scheme rf (a) or pulse scheme rf (b), is embedded in the sequence [26] displayed as the lower part of figure 3. Because homonuclear J couplings cannot be refocussed, multiplet signals demand that the duration of transverse storage be restricted, typically to a few milliseconds for protons. Hence, CIDNP has to be stored on the z axis for the rest of the time until the laser is ready to fire again (i.e. 100 ms with our system). On that timescale, the background might recover appreciably during these longitudinal storage periods S_2 . However, that recovery can be completely suppressed by inserting a grid of π pulses with a timing scheme recently developed [36] for background elimination in steady-state CIDNP experiments. (For the same reason, the echo delays surrounding the first and the second π pulse of each double echo have to be chosen marginally different.) To minimize signal losses during the longitudinal storage periods, composite inversion pulses (GROPE-16 [37]) are used.

Although the echo and inversion pulses are π pulses, they might put some CIDNP into the transverse plane, partly because of pulse non-idealities, and for rapid kinetics also because CIDNP changes during the π pulses. However, that small contamination can be eliminated by pulsed field gradients, which are shown in the figure for the transverse storage periods. Non-commensurate gradient strengths were chosen to avoid accidental refocussing of the parasitic signals; apart from that consideration, the gradient strengths and durations are not crucial.

CIDNP still evolving during the longitudinal storage period will be sampled by the next $\pi/2$ pulse (with pulse scheme rf (a)) or effective $\pi/2$ pulse (with pulse scheme rf (b)) of block S_1 . This contamination will normally be extremely small. It will be exactly zero if CIDNP generation has come to a close during the transverse storage period because all CIDNP present at the end of S_1 is destroyed; furthermore, the grid of inversion pulses during S_2 strongly suppresses polarizations developing at that stage because the periodic sign changes lead to their cancellation. If necessary, the duration of transverse storage can be increased. Even in this case, evolution under J coupling will not lead to multiplet distortions because only the in-phase components are selected by the last $\pi/2$ pulse of S_1 , and the signal losses are relatively small because the modulation amplitudes of these terms are cosine functions.

Because of the periods of transverse storage, it is perhaps not immediately obvious that the described pulse sequences are applicable to multiplet signals as well (in [26] the sensitivity improvement was demonstrated for a singlet only). As experimental proof, figure 4 displays the aromatic part of the CIDNP spectrum of 3-fluorotyrosine sensitized by flavin mononucleotide in water. A cyclic electron-transfer mechanism causes an absorptive net polarization of H^2 and an emissive one of $H^{5,6}$ in the regenerated amino acid [17]. We chose that system because it allows a direct comparison of the performance in the case of a heteronuclear J coupling (between H^2 and the fluorine nucleus) and a homonuclear J coupling (between H^5 and H^6), i.e. one J coupling that is eliminated by a spin echo and one that cannot be refocussed.

No distortions of multiplets by our multiframe sequence can be discerned in the figure. Nor does the homonuclear coupling between H^5 and H^6 cause any detectable signal losses. While a quantitative evaluation will be given below (figure 7), it is already evident from the spectra that the signals of $H^{5,6}$ increase more strongly with the number of laser flashes than those of H^2 , so the losses are actually smaller for the nuclei experiencing a homonuclear coupling.

The less surprising aspect of this good performance with multiplet signals is the negligible evolution of the non-refocussable terms during the echo delays: for a total multiplet width as in figure 4 and a typical duration of transverse storage up to one millisecond, the phase error is calculated to be smaller than $\pm 5^\circ$, so the cosine modulation should decrease the in-phase magnetization by less than 0.5%; the potentially troublesome out-of-phase terms would be much larger because of the sine modulation, but are destroyed by the gradients. Remarkable, however, is the fact that there are no artifacts caused by the strong coupling between H^5 and

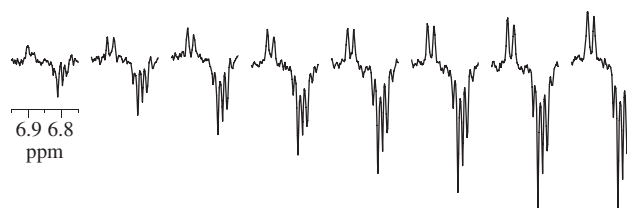


Figure 4. Multiframe photo-CIDNP experiments on a solution of 4 mM 3-fluoro-DL-tyrosine and 0.2 mM flavin mononucleotide in D_2O at pH 6.5. Shown is the aromatic region of the spectra with the absorptive doublet of H^2 (6.9 ppm) and the emissive AB multiplet of $H^{5,6}$ (6.8 ppm). The number of flashes per acquisition rises from one (left) to eight (right). Other experimental parameters, 16 acquisitions per spectrum, $\pi/2$ sampling pulses, sampling pulses immediately following the laser flashes, 100 μ s echo delay.

H^6 , which form an AB system. As is well known [38], a spin-echo pulse in such a strongly coupled spin system transfers coherence from the A to the B nuclei and *vice versa*. We will now show that the use of a *double* spin echo is the factor responsible for the absence of coherence transfer artifacts in our multiframe sequences.

The basis functions of an AB system (resonance frequencies of A and B, ν_A and ν_B ; coupling constant, J) are

$$|1\rangle = |\alpha\alpha\rangle, \quad (1)$$

$$|2\rangle = \cos\theta |\alpha\beta\rangle + \sin\theta |\beta\alpha\rangle, \quad (2)$$

$$|3\rangle = -\sin\theta |\alpha\beta\rangle + \cos\theta |\beta\alpha\rangle, \quad (3)$$

$$|4\rangle = |\beta\beta\rangle, \quad (4)$$

with

$$2\theta = \arctan \frac{J}{\nu_A - \nu_B}.$$

The single-transition shift operators $|m\rangle\langle n|$ are eigenoperators under free precession (Zeeman interaction and J coupling described by the spin Hamiltonian \mathcal{H}) during a time τ ,

$$|m\rangle\langle n| \xrightarrow{\mathcal{H}\tau} \exp\{i(\omega_n - \omega_m)\tau\} |m\rangle\langle n|, \quad (5)$$

where the frequencies ω_j are given by the diagonal elements $\langle j|\mathcal{H}|j\rangle$ of the Hamiltonian. Together with the polarization operators $|n\rangle\langle n|$ they form a complete set of basis operators; as opposed to product operators, they are also suitable for strongly coupled systems [38].

The AB spectrum is characterized by a centre frequency ω_0 and two displacement frequencies of the A lines, which enter the calculations with inverted signs for the B lines. Exploiting this symmetry, free precession during τ is describable by three phase angles χ , ϕ , and ψ , the first of which is associated with ω_0 . For the single-quantum coherences, equations (6)–(9), double-quantum coherences, equation (10), and zero-quantum coherences, equation (11), one has

$$|1\rangle\langle 2| \xrightarrow{\mathcal{H}\tau} \exp[-i\chi] \exp[+i\phi] |1\rangle\langle 2|, \quad (6)$$

$$|1\rangle\langle 3| \xrightarrow{\mathcal{H}\tau} \exp[-i\chi] \exp[-i\psi] |1\rangle\langle 3|, \quad (7)$$

$$|2\rangle\langle 4| \xrightarrow{\mathcal{H}\tau} \exp[-i\chi] \exp[-i\phi] |2\rangle\langle 4|, \quad (8)$$

$$|3\rangle\langle 4| \xrightarrow{\mathcal{H}\tau} \exp[-i\chi] \exp[+i\psi] |3\rangle\langle 4|, \quad (9)$$

$$|1\rangle\langle 4| \xrightarrow{\mathcal{H}\tau} \exp[-2i\chi] |1\rangle\langle 4|, \quad (10)$$

$$|2\rangle\langle 3| \xrightarrow{\mathcal{H}\tau} \exp[-i(\phi + \psi)] |2\rangle\langle 3|. \quad (11)$$

Interchanging the bra and the ket inverts the sign of the argument of each exponential on the right-hand side of the respective equation. The polarization operators $|n\rangle\langle n|$ have no time dependence.

Only in the product basis, thus for weakly coupled spin systems, does a π pulse always transform one basis operator $|m\rangle\langle n|$ into another, for example $|\alpha\alpha\rangle\langle\alpha\beta|$ into $|\beta\beta\rangle\langle\beta\alpha|$. For strongly coupled systems, some basis functions are superpositions of product functions, and a π pulse causes a mixed transformation of basis operators, for example in the AB system

$$|1\rangle\langle 2| \xrightarrow{\pi_x} c |4\rangle\langle 3| + s |4\rangle\langle 2|, \quad (12)$$

with c and s as abbreviations for $\cos 2\theta$ and $\sin 2\theta$ (compare equations (2) and (3)). The effects of a preceding and a subsequent free precession period follow from equations (6), (8), and (9). The result for a single spin echo $\tau - \pi_x - \tau$ is thus

$$|1\rangle\langle 2| \xrightarrow{\tau - \pi_x - \tau} \cos[\phi - \psi] c |4\rangle\langle 3| + \cos[2\phi] s |4\rangle\langle 2|, \quad (13)$$

where the imaginary part was omitted because it is out of phase with the initial coherence. It is evident that coherence is transferred not only into the parallel transition, as in the case of a weakly coupled system ($\theta = 0$), but also into the connected transition. This makes a single spin-echo block useless for transverse storage of a strongly coupled CIDNP signal.

However, with a double spin echo that problem is removed, or at least greatly alleviated. For the AB system, the single-quantum coherences resulting from the first pulse are transformed by another π pulse according to

$$|4\rangle\langle 3| \xrightarrow{\pi_x} c |1\rangle\langle 2| - s |1\rangle\langle 3|, \quad (14)$$

$$|4\rangle\langle 2| \xrightarrow{\pi_x} s |1\rangle\langle 2| + c |1\rangle\langle 3|. \quad (15)$$

When two such pulses are combined without surrounding evolution periods, i.e. for a double spin-echo block with $\tau \rightarrow 0$, the transfer factors from $|1\rangle\langle 2|$ to the connected single-quantum coherence $|1\rangle\langle 3|$ exactly cancel because they have identical magnitudes but opposite signs for the two pathways, via $|4\rangle\langle 2|$ or via $|4\rangle\langle 3|$. In contrast, the transfer factors back to the starting single-quantum coherence add up to unity. This result is not surprising because two π pulses in succession amount to a full rotation; for that reason its validity is neither restricted to an AB system nor dependent on the symmetry of the spin system.

n spins: owing to the above-mentioned independent transformation, equation (23) holds for each spin in the product operator, so in the resulting sum all terms containing one or more y operators vanish, and the only remaining term is the starting product operator $2^{n-1} \prod_{i=1}^n \mathbf{I}_{ix}$.

When the product operator further contains m longitudinal operators, the outcome depends on m because each longitudinal operator is inverted by the π pulse. Normal refocussing occurs when m is even, but refocussing is accompanied by inversion when m is odd. We mention for completeness that product operators containing terms \mathbf{I}_{iy} —which do not arise with the pulse phases given in figure 3—would behave in an analogous manner because each such term is refocussed with inversion. However, the application of two spin-echo blocks in succession, which are part of our pulse sequences of figure 3, will undo all these inversions. In other words, a double-spin echo leaves unchanged all product operators composed of an arbitrary number of longitudinal and/or transverse operators, as long as there is no evolution due to J coupling.

Because the last pulse of the block S_1 is a $\pi/2$ pulse of phase \bar{y} , the only product operators it selects for longitudinal storage are $2^{n-1} \prod_{i=1}^n \mathbf{I}_{ix}$; all product operators containing one or more longitudinal operators before that final pulse are converted into product operators containing one or more transverse operators, which are destroyed by the subsequent spoiling gradient. The multiflash experiments of figure 3 thus select exactly one transfer pathway, namely

$$\begin{array}{ccc}
 2^{n-1} \prod_{i=1}^n \mathbf{I}_{iz} & \xrightarrow{\sin^n \alpha} & 2^{n-1} \prod_{i=1}^n \mathbf{I}_{ix} & \xrightleftharpoons[1]{1} & 2^{n-1} \prod_{i=1}^n \mathbf{I}_{iz} \\
 \text{CIDNP} & & \text{transverse} & & \text{longitudinal} \\
 \text{generation} & & \text{storage} & & \text{storage} \\
 & & & & \xrightarrow{\sin \varphi \cos^{n-1} \varphi} & 2^{n-1} \prod_{i=1}^n (\mathbf{I}_{ix} + \mathbf{I}_{iz}) \\
 & & & & & \text{readout}
 \end{array} \quad (24)$$

For simplicity, the phase of the readout pulse was assumed to be y ; if it were x instead, \mathbf{I}_{ix} in the last term of equation (24) would have to be replaced by $-\mathbf{I}_{iy}$.

The transfer amplitudes have also been included in equation (12). At the end of S_1 , the transverse signal is restored to the z axis by a $\pi/2$ pulse; likewise, CIDNP already stored on the z axis is restored to the transverse plane either by a single $\pi/2$ pulse (in the basic sequence, i.e. S_1 only) or by a composite $\pi/2$ pulse with intervening double-spin echo (in the more sophisticated version, i.e. S_0 plus S_1). Hence, the transfer amplitude for the restoring process in either direction is unity (i.e. $\sin^n \pi/2$) regardless of the number n of spins in the product operator. The initial observation pulse converts

CIDNP n -spin order into n -spin coherence, so the pertaining transfer amplitude is $\sin^n \alpha$. For small flip angles α , this leads to a strong suppression of higher spin orders. However, we stress that with the basic sequence that transfer amplitude becomes unity for *all* spin orders because a $\pi/2$ pulse is used for observation; this is in strong contrast to normal sampling of multiplet CIDNP, for which the transfer pathway is that induced by the very last pulse of our overall sequence (lower part of figure 3). Hence, a separation of the different spin orders can be performed in the usual way, by the flip angle φ of that readout pulse. The associated transfer amplitude is $\sin \varphi \cos^{n-1} \varphi$, because only product operators containing a single transverse operator evolve into an observable signal during the acquisition period.

Experimental proof that transverse and longitudinal storage of a CIDNP multiplet effect is possible in the same way as for a CIDNP net effect is given in figure 5. For this, pure two-spin order was generated by the following pulse sequence acting on the aromatic protons of tyrosine, which at 600 MHz form an apparent AX spin system,

$$\begin{aligned}
 \mathbf{I}_{1z} + \mathbf{I}_{2z} &\xrightarrow{(\pi/2)_y} \mathbf{I}_{1x} + \mathbf{I}_{2x} \xrightarrow{1/(8J) - \pi_x - 1/(4J) - \pi_x - 1/(8J)} 2\mathbf{I}_{1y}\mathbf{I}_{2z} \\
 &+ 2\mathbf{I}_{1z}\mathbf{I}_{2y} \xrightarrow{(\pi/4)_x} 2\mathbf{I}_{1z}\mathbf{I}_{2z} - 2\mathbf{I}_{1y}\mathbf{I}_{2y} \xrightarrow{G_z} 2\mathbf{I}_{1z}\mathbf{I}_{2z},
 \end{aligned} \quad (25)$$

The resulting two-spin order $2\mathbf{I}_{1z}\mathbf{I}_{2z}$ (i.e. multiplet effect) can be observed by the usual procedure: spectra with $\pi/4$ and $3\pi/4$ observation pulses are recorded; their subtraction adds the multiplet effect constructively and suppresses any residual one-spin order (i.e. net effects) that might have been caused by pulse non-idealities. The spectrum labeled '0' in figure 5 displays the outcome of that control experiment for the low-field doublet, which exhibits the antiphase structure typical for a CIDNP multiplet effect. Next, one or several transverse plus longitudinal storage blocks ($S_1 + S_2$) were inserted



Figure 5. Storage of two-spin order in a spin system. Shown is the high-field doublet of the aromatic protons (ca. 8.5 ppm) of L-tyrosine (4 mM in D_2O ; 16 acquisitions per spectrum). Two-spin order was generated by the pulse sequence of equation (25), subjected to the number of storage cycles ($S_1 + S_2$) given at the traces, and then read out by a pulse. The spectrum labeled '0' is the control experiment without storage. Further explanation, see text.

between the generating sequence (equation (25)) and the readout pulse. Apart from the expected (see the analysis below) slow decrease of the amplitudes with increasing storage time and some insignificant line broadening, this does not cause any changes of the signal shapes, as can be seen in the figure. Hence, this experiment demonstrates the feasibility of storing multiplet effects without distortions by our pulse sequence.

Finally, experimental proof of the applicability of our multflash pulse sequences to a true CIDNP multiplet effect is provided by figure 6. When β -NADH (nicotine adenine dinucleotide) is sensitized with a flavin dye in air-saturated solution, H^4 and H^4' exhibit very strong A/E polarizations at 360 MHz [41]; again, these CIDNP signals are due to a cyclic electron transfer. With our current equipment the magnetic field is higher by some 60% and the accessible light intensities are about 80 times lower compared with [41], so the CIDNP intensities are weaker by almost two orders of magnitude, thus making the signal enhancement by the multflash method very desirable. As is immediately obvious from figure 6, our pulse sequences lead to undistorted CIDNP multiplet effects and a signal increase that is clearly stronger than the square root of the number of flashes n , at least for n up to four. (See below for a detailed analysis of the effect of storage losses on the performance).

H^4H^4' are still strongly coupled even at 600 MHz, so the intensities of the outer and inner multiplet lines are not identical, as they would be for an AX system, but depend on the ratio θ , which was defined following equations (1)–(4). However, the flip angle dependence is the same as in the case of weak coupling ($1/2 \sin 2\alpha$), as can be derived from the formulae given in [42], so the

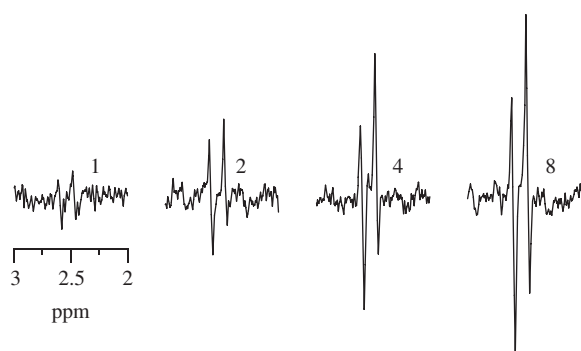


Figure 6. Multiflash time-resolved CIDNP experiments on a system exhibiting a multiplet effect. Solution, 2 mM β -NADH (nicotine adenine dinucleotide) sensitized by 0.1 mM flavin mononucleotide in D_2O at pH 10.04. The number of flashes is given at the traces, '1' denoting the control experiment with a single flash. Laser flash preceding the sampling pulse by 10 μ s, 100 μ s echo delay, eight acquisitions per spectrum. Further explanation, see text.

usual subtraction of two spectra, one obtained with a $\pi/4$ pulse, the other with a $3\pi/4$ pulse, yields the pure CIDNP multiplet effect and suppresses the CIDNP net effect.

In the described multflash experiments, the signal should ideally increase linearly with the number of flashes n , but storage losses will spoil this linear increase. Nuclear spin relaxation is the predominant source of such losses [26], because in an n -flash experiment CIDNP has to be stored, on average, for $n/2$ times the repetition period of the laser, which amounts to $n \times 50$ ms in our case. Lasers capable of firing much more rapidly are commercially available, so that is not a true limitation of the method; however, as a caveat we mention that excessively high repetition rates might cause line broadening due to sample heating. Pulse imperfections, which are a second source of losses, do not play a decisive role with modern NMR spectrometers.

Because each storage cycle has the same duration and contains the same number of rf pulses, the same relative amount of the stored signal is lost by it. Hence, the efficiency of each cycle is describable [26] by the same factor b , $0 \leq b \leq 1$, which only depends on the laser repetition period t_{rep} and an effective relaxation time $T_{1,\text{eff}}$ (which also takes into account any refocussing non-idealities),

$$b = \exp\left(\frac{-t_{\text{rep}}}{T_{1,\text{eff}}}\right). \quad (26)$$

Assuming that each flash yields the same CIDNP signal σ and that one acquisition incurs the noise ν , the signal-to-noise ratio S/N is obtained [26] by summing up a geometric series,

$$\frac{S}{N} = \frac{\sigma}{\nu} \sum_{j=1}^n b^j = \frac{\sigma}{\nu} \cdot \frac{b(1-b^n)}{(1-b)}. \quad (27)$$

Figure 7 compares the results obtained by the multflash method for the aromatic protons of 3-fluorotyrosine (see figure 4) with the theoretical curve for signal averaging in the conventional way,

$$\frac{S}{N} = \frac{\sigma}{\nu} \cdot \sqrt{n}. \quad (28)$$

Taking a point on the latter curve as a point of reference, the multflash sequences either yield a sensitivity that is higher with the same number of flashes (as the vertical arrow indicates) or allow one to obtain the same sensitivity with fewer flashes (as illustrated by the horizontal arrow).

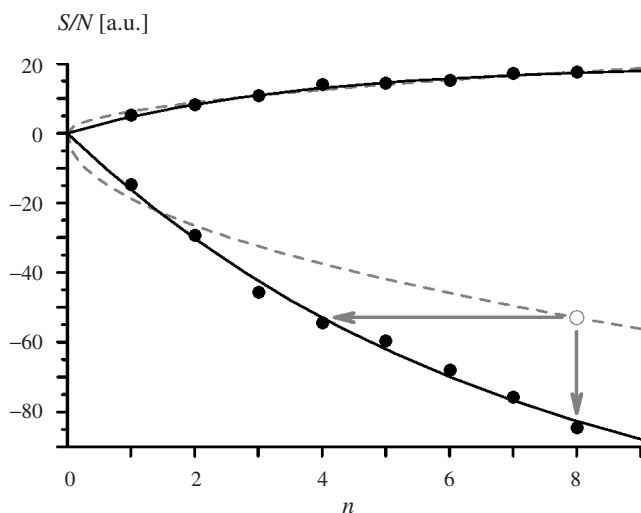


Figure 7. Sensitivity S/N as a function of the number of flashes n for the experiment of figure 4. Positive and negative data points, integrals over the signals of H^2 and $H^{5,6}$, respectively. The solid lines display the best fits of equation (27) to the two data sets (H^2 , $\sigma/\nu = 6.23$, $b = 0.76$; $H^{5,6}$, $\sigma/\nu = -18.7$, $b = 0.87$). The dashed lines are the theoretical curves for conventional signal averaging, equation (28). The open circle and arrows show the point of reference and the two applications of the multiflash sequences, sensitivity increase or reduction of the absorbed light.

Because $b(1 - b^n)/(1 - b)$ is a convex function, the second effect will always be larger.

The actual improvement is determined by the factor b . An example is again provided by 3-fluorotyrosine. The effective relaxation time of H^2 is shorter than that of $H^{5,6}$ because of the adjacent fluorine nucleus, resulting in a smaller value of b . As is clearly seen in figure 7, the multiflash sequence yields no improvement over conventional signal averaging in the case of H^2 —apart from the strongly reduced duration of the experiment, by a factor of n —but a significant one in the case of $H^{5,6}$. In the following, we will analyse the influence of b on the performance in more detail.

For a given number n of flashes, the sensitivity gain G relative to signal averaging in the conventional way is calculated from equations (27) and (28) to be

$$G = \frac{b(1 - b^n)}{(1 - b)\sqrt{n}}. \quad (29)$$

This expression has been plotted in figure 8 for different values of the efficiency b . Also included in the figure is the theoretical limiting curve for $b \rightarrow 1$, i.e. \sqrt{n} . As expected, the curves for $b < 1$ all lie below the limiting curve. Moreover, they all pass through a maximum because the sum of the geometric series converges

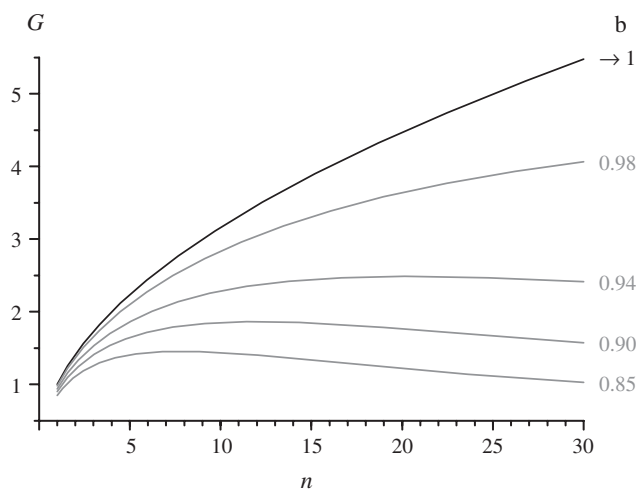


Figure 8. Sensitivity gain G , calculated by equation (29), of a multiflash sequence relative to conventional signal averaging as a function of the number of laser flashes n for different values of the storage efficiency b .

towards an upper limit, whereas \sqrt{n} in the denominator increases without bounds. With decreasing b , the position of the maximum shifts to smaller n and its height decreases. This has two consequences. First, for given b there is a maximum useful number of flashes above which the sensitivity gain decreases again. Second, there is a minimum efficiency below which the maximum height is smaller than unity, i.e. below which the multiflash sequence will yield a lower sensitivity than conventional signal averaging. That minimum value is found to be 0.75, which is very close to the experimental result for H^2 in 3-fluorotyrosine.

The maximum sensitivity gain G_{\max} as a function of b was determined numerically because a closed-form solution is unavailable. Figure 9 displays the resulting curve. The increasingly steep rise as b approaches unity reflects the fact that, in this regime, the maximum occurs increasingly late, i.e. at an increasingly higher number of flashes, with concomitant rise of the sensitivity gain. Significant but not spectacular sensitivity gains ($G_{\max} \leq 3.6$) are achieved for realistic efficiency parameters ($b \leq 0.97$, compare [26]).

Division of G_{\max} by the square root of the—again numerically determined—number of flashes needed to obtain that maximum value shows how closely the theoretical limit of the improvement can be approached. As is seen in figure 10, that ratio depends only weakly on b and is slightly higher than 0.5 throughout the whole range of b . Hence, approximately one-half of the theoretical sensitivity gain is obtainable.

Inverting equation (27) such that the number of flashes becomes the dependent variable, inserting equation (28), taking the reciprocal of the result, and

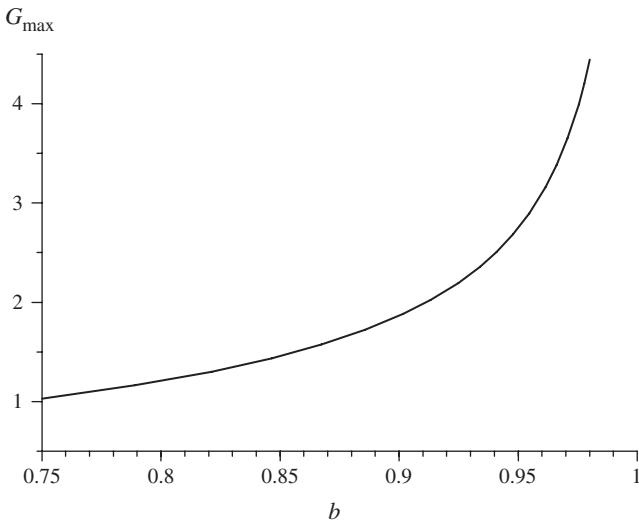


Figure 9. Numerically obtained maximum sensitivity gain G_{\max} , relative to conventional signal averaging, as a function of the efficiency b .

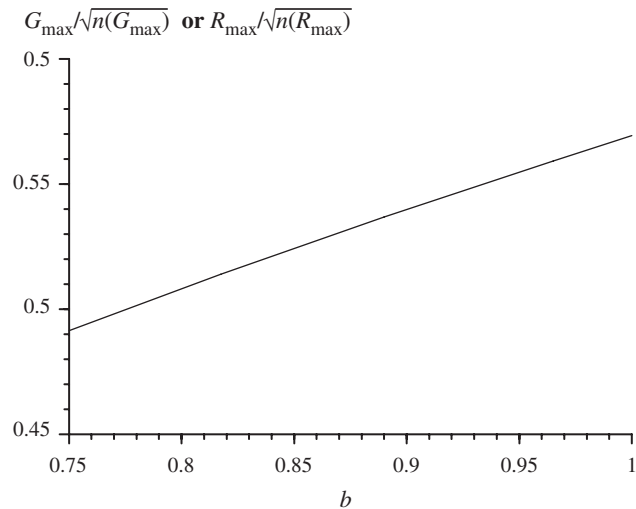


Figure 10. Fraction $G_{\max}/[n(G_{\max})]^{1/2}$ of the maximum theoretical sensitivity gain, or fraction $R_{\max}/[n(R_{\max})]^{1/2}$ of the maximum reduction of absorbed light, that are accessible for given efficiency b .

multiplying the final expression by n gives the reduction R of the light intensity that can be achieved with the multiflash sequences,

$$R = \frac{n \ln b}{\ln[1 - \sqrt{n}(1/b - 1)]}. \quad (30)$$

A plot of that function for the same values of the parameter b as before is displayed in figure 11, together with the theoretical limiting curve for $b \rightarrow 1$, i.e. \sqrt{n} . The general shape of the curves is similar to those of

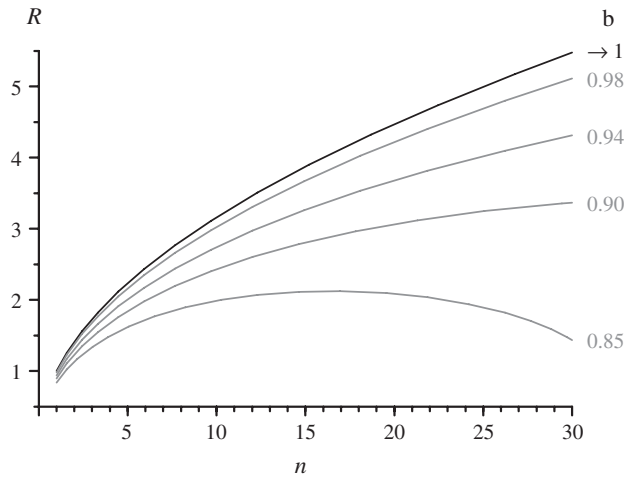


Figure 11. Reduction R of the absorbed light by the multiflash experiments as a function of the number n of flashes in a conventional signal-averaging experiment, with the efficiency b as parameter.

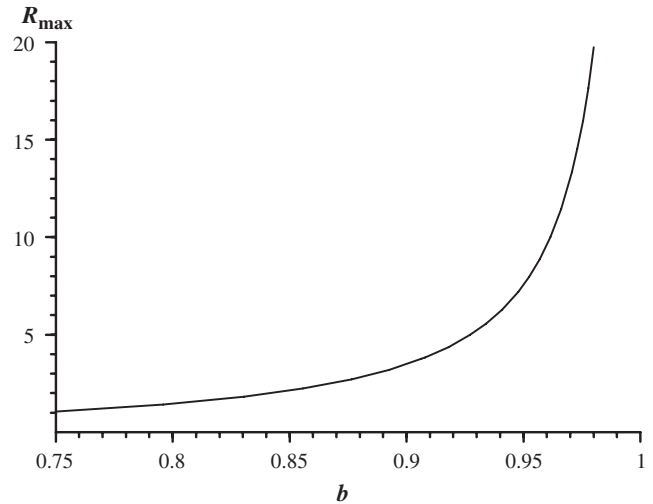


Figure 12. Numerically obtained maximum reduction R_{\max} of the absorbed light, compared with conventional signal averaging, by the multiflash experiments as a function of the efficiency b .

figure 8 but they are seen to lie much closer to the limiting curve, as is to be expected because fewer storage cycles are needed for that kind of improvement. However, the same value of b as in the previous case, $b = 0.75$, constitutes the minimum storage efficiency below which the multiflash sequences yield no advantage compared with conventional signal averaging.

The maximum achievable reduction R_{\max} of the number of flashes was again determined numerically, and has been plotted as a function of b in figure 12. Dividing R_{\max} by the square root of the number of flashes needed one obtains exactly the same curve as in

figure 10 despite the different functional forms of equations (29) and (30). Hence, with both applications, approximately one-half of the theoretical limit of the improvement can be reached.

The shape of the curve for R_{\max} is similar to that for G_{\max} , but comparison of the vertical scales of figures 9 and 12 shows that the achievable reduction of the absorbed light is much stronger than the achievable signal increase (with $b = 0.97$ [26], by a factor of 13 for the former, as opposed to 3.6 for the latter).

4. Conclusions

The multflash pulse sequences described in this work address the key problem of time-resolved CIDNP spectroscopy, i.e. the sensitivity of the experiment. As their central idea, the desired and unwanted signal components are stored in different observables (transverse and z magnetization) and exchanged between them in such a way that the desired component is accumulated and the undesired one destroyed. The experimental examples and theoretical analysis have shown that multiplet signals are neither distorted nor reduced in their intensity, and that strong coupling does not adversely affect the performance. The sequences are not only applicable to CIDNP net effects but also to CIDNP multiplet effects.

As to their optimization, we arrive at three guidelines. First, time-resolved measurements of CIDNP multiplet effects should always be performed with the basic sequence (figure 3, trace rf (a)), which uses $\pi/2$ pulses for storage; for CIDNP net effects, both sequences are suited equally well. Second, the performance is determined by a single parameter, the storage efficiency b (equation (26)). There is a minimum value of b (0.75) below which the sequences will give no advantage compared with conventional signal averaging; the nearer to unity b lies, the larger the improvement becomes. To maximize b , the laser repetition rate should be chosen as fast as the equipment and experimental limitations permit. By experiments as shown in figure 5, b can be measured before starting the actual CIDNP experiments, thus allowing one to choose conditions best suited for the system under study. Third, concerning the two uses, sensitivity increase or reduction of the absorbed light, the latter is always the larger effect.

References

- [1] J. Bargon, H. Fischer, and U. Johnsen, *Z. Naturf. (a)* **22**, 1551 (1967).
- [2] H. R. Ward and R. G. Lawler, *J. Am. Chem. Soc.* **89**, 5518 (1967).
- [3] See, e.g., M. Goez, in *Advances in Photochemistry*, edited by D. C. Neckers, D. H. Volman, and G. von Büнау (Wiley, New York, 1997), Vol. 23, p. 63, and references therein.
- [4] T. Aizawa, T. Sakata, S. Itoh, K. Maeda, and T. Azumi, *Chem. Phys. Lett.* **195**, 16 (1992).
- [5] M. V. Fedin, E. G. Bagryanskaya, and P. A. Purtov, *J. Chem. Phys.* **111**, 5491 (1999).
- [6] Y. P. Tsentalovich, O. B. Morozova, N. I. Avdievich, G. S. Ananchenko, A. V. Yurkovskaya, J. D. Ball, and M. D. E. Forbes, *J. Phys. Chem. A* **101**, 8809 (1997).
- [7] A. Yurkovskaya, S. Grosse, S. Dvinskikh, O. Morozova, and H.-M. Vieth, *J. Phys. Chem. A* **103**, 980 (1999).
- [8] M. Goez and J. Rozwadowski, *J. Phys. Chem. A* **102**, 7945 (1998).
- [9] M. Goez and I. Frisch, *J. Phys. Chem. A* **106**, 8079 (2002).
- [10] G. Pohlers, H. Dreeskamp, and S. Grimme, *J. Photochem. Photobiol. A* **95**, 41 (1996).
- [11] G. Eckert and M. Goez, *J. Am. Chem. Soc.* **121**, 2274 (1999).
- [12] S. N. Batchelor and H. Fischer, *J. Phys. Chem.* **100**, 9794 (1996).
- [13] M. Goez and I. Sartorius, *J. Phys. Chem. A* **107**, 8539 (2003).
- [14] M. G. Zysmilich and A. McDermott, *J. Am. Chem. Soc.* **118**, 5867 (1996).
- [15] E. A. M. Schulten, J. Matysik, Alia, S. Kiihne, J. Raap, J. Lugtenburg, P. Gast, A. J. Hoff, H. J. M. deGroot, and J. M. Huub, *Biochem.* **41**, 8708 (2002).
- [16] C. E. Lyon, J. A. Jones, C. Redfield, C. M. Dobson, and P. J. Hore, *J. Am. Chem. Soc.* **121**, 6505 (1999).
- [17] K. H. Mok and P. J. Hore, *Methods* **34**, 75 (2004), and references therein.
- [18] G. L. Closs, *J. Am. Chem. Soc.* **91**, 4552 (1969).
- [19] R. Kaptein and L. J. Oosterhoff, *Chem. Phys. Lett.* **4**, 195 (1969).
- [20] O. B. Morozova, A. V. Yurkovskaya, Y. P. Tsentalovich, M. D. E. Forbes, P. J. Hore, and R. Z. Sagdeev, *Molec. Phys.* **100**, 1187 (2002).
- [21] A. V. Yurkovskaya, O. A. Snytikova, O. B. Morozova, Y. P. Tsentalovich, and R. Z. Sagdeev, *Phys. Chem. Chem. Phys.* **17**, 3653 (2003).
- [22] O. B. Morozova, A. V. Yurkovskaya, H.-M. Vieth, and R. Z. Sagdeev, *J. Phys. Chem. B* **107**, 1088 (2003).
- [23] O. B. Morozova, S. E. Korchak, A. V. Yurkovskaya, and R. Z. Sagdeev, *J. Phys. Chem. A* **109**, 10459 (2005).
- [24] O. B. Morozova, A. V. Yurkovskaya, and R. Z. Sagdeev, *J. Phys. Chem. B* **109**, 3668 (2005).
- [25] O. B. Morozova, P. J. Hore, R. Z. Sagdeev, and A. V. Yurkovskaya, *J. Phys. Chem. B* **109**, 21971 (2005).
- [26] M. Goez, I. Kuprov, and P. J. Hore, *J. Magn. Reson.* **177**, 139 (2005).
- [27] I. Kuprov, M. Goez, P. A. Abbott, and P. J. Hore, *Rev. Scient. Instrum.* **76**, 084103/1 (2005).
- [28] S. Schäublin, A. Wokaun, and R. R. Ernst, *J. Magn. Reson.* **27**, 273 (1977).
- [29] G. L. Closs and R. J. Miller, *J. Am. Chem. Soc.* **101**, 1639 (1979).
- [30] Y. P. Tsentalovich, A. V. Yurkovskaya, and R. Z. Sagdeev, *J. Photochem. Photobiol. A* **70**, 9 (1993).
- [31] M. Goez and V. Zubarev, *Chem. Phys.* **256**, 107 (2000).
- [32] H. Y. Carr and E. M. Purcell, *Phys. Rev.* **94**, 630 (1954).
- [33] S. Meiboom and D. Gill, *Rev. Scient. Instrum.* **29**, 93 (1958).

- [34] M. Goetz, *J. Magn. Reson. A* **123**, 161 (1996).
- [35] M. Goetz, *Chem. Phys. Lett.* **165**, 11 (1990).
- [36] M. Goetz, K. Hun Mok, and P. J. Hore, *J. Magn. Reson.* **177**, 236 (2005).
- [37] A. J. Shaka and R. Freeman, *J. Magn. Reson.* **55**, 487 (1983).
- [38] R. R. Ernst, G. Bodenhausen, and A. Wokaun, *Principles of Nuclear Magnetic Resonance in One and Two Dimensions* (Clarendon Press, Oxford, 1987).
- [39] R. Hany, J.-K. Vollenweider, and H. Fischer, *Chem. Phys.* **120**, 169 (1988).
- [40] O. W. Sørensen, G. W. Eich, M. H. Levitt, G. Bodenhausen, and R. R. Ernst, *Prog. NMR Spectrosc.* **16**, 163 (1983).
- [41] P. J. Hore, A. Volbeda, K. Dijkstra, and R. Kaptein, *J. Am. Chem. Soc.* **104**, 6262 (1982).
- [42] S. Schäublin, A. Höhener, and R. R. Ernst, *J. Magn. Reson.* **13**, 196 (1974).